



Effect of ash removal on structure and pyrolysis/gasification reactivity of a Chinese bituminous coal

Qing He¹ · Yan Gong¹ · Lu Ding¹ · Xingjun Wang¹ · Guangsuo Yu^{1,2}

Received: 28 February 2020 / Revised: 25 April 2020 / Accepted: 21 July 2020 / Published online: 3 August 2020
© The Author(s) 2020

Abstract In this study, the effect of ash removal on Shenfu bituminous coal was investigated. The coal was pretreated by hydrofluoric acid (HF) pickling, and the raw/pretreated coal chars were prepared at 900 °C in a fixed bed reactor. The structure of coal and char were detected by Fourier transform infrared (FTIR) and Raman spectroscopy. The reactivity was tested in a thermogravimetric analyzer, including coal pyrolysis and char gasification. The reaction kinetics was analyzed through the Coats–Redfern method, master plots, the model-free and model-fitting method. The results show that the HF pickling can remove silicon from coal efficiently, and the macromolecular framework of coal is quite stable according to FTIR. The Raman parameters imply some carbonaceous structure on coal surface changed. For slow pyrolysis of coal, the effect of heating rate is considered. The changes of pyrolysis characteristics and kinetics are insignificant. For char gasification, the reactivity under isothermal and non-isothermal condition are discussed with an emphasis in different residence time of devolatilization process. In kinetic control region (low temperature), the activation energy (E_a) is very close (about 240 kJ/mol) for all chars. With the temperature increases, the reactivity of raw coal char is more easily suffered by diffusion. The random pore model is more suitable for the ash-free coal char, and the char with long residence time has a larger value of structural parameter ψ and smaller value of pre-exponential factor A . The E_a calculated by model-fitting and model-free method were in good agreement.

Keywords Gasification · Pyrolysis · Demineralization · Kinetics · Structure evolution · Master plot

Electronic supplementary material The online version of this article (<https://doi.org/10.1007/s40789-020-00353-w>) contains supplementary material, which is available to authorized users.

✉ Lu Ding
dinglu@ecust.edu.cn

✉ Guangsuo Yu
gsyu@ecust.edu.cn

¹ Institute of Clean Coal Technology, East China University of Science and Technology, Shanghai 200237, China

² State Key Laboratory of High-Efficiency Utilization of Coal and Green Chemical Engineering, Ningxia University, Yinchuan 750021, Ningxia, China

1 Introduction

Coal is the main irreplaceable resource in current and future energy system, especially in China. Clean and efficient use of coal is an effective measure to control greenhouse gas emissions and reduce environmental pollution. At present, combustion, gasification and pyrolysis are the main utilization of coal (Cui et al. 2014; Mishra et al. 2018). Recently, some new concepts of coal utilization have been proposed, e.g. the oxy-coal combustion steam system (OCCSS) (Zhao et al. 2019), the integrated gasification combined cycle (IGCC) (Lin et al. 2019), ultra clean coal (UCC) production (Jorjani et al. 2011; Royaei et al. 2012), coal-topping process (Zhu et al. 2008), etc. The demineralized coal without producing the solid wastes is preferred for the advanced processes (Zhao et al. 2019). Besides, the ash-free coal features the swelling behavior,

which could be used as the binder in coke production (Kim et al. 2018). It was also reported that the ash-free coal had the potential of higher heating output, high surface area and abundant surface oxygen functional groups, which could be used to direct carbon fuel cells (Vu and Lee 2016). The reactivity change and structure evolution of the ultra clean coal/char have attracted more and more attention among researchers.

Coal ash is an important component of coal and has a significant influence on the reactivity. Recently, Ning et al. studied the correlation between the ash content and structure/reativity of coal, including the bituminous and anthracite (Ning et al. 2019). Coal ash usually contains some alkali and alkaline earth metals (AAEMs) as well as the silicon. It is reported that AAEMs work catalytically for gasification (Ban et al. 2019; Mi et al. 2015). For example, Ca could accelerate the gasification at the initial stage, whereas the Na or K have obvious catalytic effect on gasification at the late stage (Kramb et al. 2017; Zhang et al. 2010). This indicates that the ash-free coal char may have a lower gasification reactivity. At the same time, the ash would increase the intra-particle transfer resistance of the agent and products (Ding et al. 2014, 2017). Whereas the physical opening of coal structure by ash removal could make it easier for the gasifying agent to diffuse into the structure (Strydom et al. 2011). These suggest the ash-free coal char may have a higher reactivity. Therefore, the effect of ash on gasification reactivity needs to be further clarified.

The gasification kinetics is an important aspect for research (Gao et al. 2016; Lin and Strand 2013). Many kinetic models are derived without considering the effect of ash (Irfan et al. 2011). For example, the random pore model (RPM) takes the growth and coalescence/overlapping of pores into consideration (Mahinpey and Gomez 2016). The model-fitting method using these models, like RPM, is widely reported in the field of coal gasification (Everson et al. 2008; Iwaszenko et al. 2019). However, the impact of coal ash is ignored in some cases. In-depth investigation about the effect of ash on kinetics parameters should be conducted. On the other hand, the gasification of pyrolysis char is the rate control step in the whole process of coal gasification. Many researches about gasification using pyrolysis char as the raw materials, and ignore the pyrolysis process (Bai et al. 2018; Jayaraman et al. 2017). However, as a pre-reaction of gasification, pyrolysis directly affects the physicochemical structure of char and indirectly determines the gasification reactivity. It is also necessary to investigate the effect of ash on pyrolysis characteristics.

In studying the effect of demineralization on pyrolysis and gasification, three steps of acid pretreatment (HCl–HF–HCl) is adopted (He et al. 2017). However, little attention

is paid with respect to the HF treatment alone. In this paper, the effect of ash removal by HF picking on coal structure and reactivity were investigated. The detailed kinetic analyses were carried out. The chemical structures of coal and char were also detected, including the surface morphology, functional group and carbonaceous structure. These data can provide experimental support for the fundamental research of coal gasification.

2 Materials and methods

2.1 Sample preparation

2.1.1 Coal demineralization

Shenfu (SF) coal was used in this study, which is a typical Chinese bituminous coal and widely used in research (Shui et al. 2011). The coal sample was ground and sieved to $\sim 100 \mu\text{m}$. The proximate and ultimate analyses of SF coal were summarized in Table 1 according to Chinese standards of GB/T 212–2008 and GB/T 31391–2015. The main composition of SF coal ash was listed in Table 2 based on GB/T 1574–2007. The demineralized (ash-free) coal was prepared by HF picking alone. Approximately 200 mL HF was added to wash 20 g bituminous coal. The mixture was stirred continuously for 48 h at room temperature. Then, the acid-pretreated sample was filtered and cleaned with deionized water. After that, the sample was dried at 105 °C to a constant weight in oven. The acid-pretreated coal was denoted as the SF-ap.

2.1.2 Char preparation

The coal chars from the raw and demineralized coal were prepared in a fixed bed reactor (hanging basket type), which could achieve a high heating rate (He et al. 2019b). The devolatilization temperature was 900 °C. In this work, the effect of residence time was taken into consideration. The devolatilization time was set at 5 and 30 min, representing a short and long reaction time. The chars prepared under short time were denoted as SF-cs and SF-ap-cs. The chars with long residence time named as SF-cl and SF-ap-cl.

2.2 Structure of coal/char

2.2.1 FTIR spectroscopy

The functional groups in raw and pretreated coal were detected by Fourier transform infrared (FTIR) spectrometer (Thermo Scientific Nicolet iS50 spectrometer). The KBr pellet method was used in the present work. Dried KBr

Table 1 Proximate and ultimate analyses of SF coal

Sample	Proximate analysis (wt%, d)			Ultimate analysis (wt%, daf)				
	A	V	FC	C	H	O*	N	S
SF	8.68	29.9	61.42	81.57	4.41	12.47	0.95	0.60

d dry basis, daf dry ash-free basis

*By difference

Table 2 Ash composition of SF coal (wt%)

Sample	SiO ₂	Al ₂ O ₃	CaO	MgO	Na ₂ O	K ₂ O	Fe ₂ O ₃	P ₂ O ₅
SF	29.03	17.33	19.2	6.63	1.23	0.78	6.73	0.07

powder was milled with coal samples at the ratio of 100:1. Then, the fine powder was compressed into a thickness pallet. The FTIR spectroscopy with the scan range of 400–4000 cm⁻¹ at a resolution of 4 cm⁻¹ was recorded for analysis.

2.2.2 Raman spectroscopy

The carbonaceous structures of coal and char were analyzed by Raman spectroscopy (Thermo Scientific DXR). The wavenumber range of 800–2000 cm⁻¹ was collected. In order to reduce the experimental error, five particles were randomly selected for test. The spectrum peaks were resolved into ten Gaussian band. A detailed description of the peak-fitting method has been given previously (He et al. 2019b).

2.2.3 Surface morphology

The surface morphology of coal, char and gasified semi-char were visually observed by microscopies, including optical microscopy (Leica) and scanning electron microscopy (SEM, Hitachi SU-1510).

2.3 Reactivity of coal/char

The reactivity of coal and char were studied in a thermogravimetric analyzer (NETZSCH STA449 F3), including coal pyrolysis and char gasification. In each run, about (8.00 ± 0.20) mg coal/char were loaded into an Al₂O₃ crucible to go through reaction with programmed temperature in different atmospheres.

2.3.1 Slow pyrolysis

Non-isothermal method was adopted for coal slow pyrolysis. The pyrolysis experiments were performed under N₂

atmosphere with the flow rate of 80 mL/min. The temperature raised from room temperature to 900 °C with the heating rates of 20 and 30 °C/min, respectively.

2.3.2 Gasification

The char gasification properties were studied under both isothermal and non-isothermal conditions. For isothermal condition, the gasification temperatures were set at 800, 850, 900, 950 and 1000 °C, respectively. To reach the desired temperature, the char had to be heated in N₂ atmosphere. Then, CO₂ was introduced with the flow rate of 120 mL/min until the gasification completed. For non-isothermal condition, the main steps were similar to that of the slow pyrolysis. The heating rate was 5 °C/min, and the purge gas was CO₂ instead of N₂.

2.3.3 Data analysis

Pyrolysis and gasification are both gas–solid heterogeneous reactions. In addition, the reactions are both taken place in a TGA in this study. Therefore, some steps of data processing and methods of kinetics analysis are similar. Firstly, the conversion X is calculated by the following formula

$$X = \frac{w_0 - w_t}{w_0 - w_f} \quad (1)$$

where, w_0 , w_t and w_f are the initial, instantaneous and final mass of the sample during reaction, respectively. The gas–solid reaction can be expressed as the function of temperature and conversion, and the temperature term follows the Arrhenius's formula

$$\begin{aligned} \frac{dX}{dt} &= k(T)f(X) \\ &= A \exp\left(-\frac{E_a}{RT}\right)f(X) \end{aligned} \quad (2)$$

where A is the pre-exponential factor, E_a is the activation energy, R is the gas constant (8.3145 J/(mol·K)), and $f(X)$ is a physical model related to conversion. The specific kinetic analysis will be briefly introduced in Sect. 3 before the detailed discussion.

3 Results and discussion

3.1 Structure evolution

Figure 1 shows the morphological characteristics of coal, char and gasified semi-char, where the chars were SF-cs and SF-ap-cs, and the gasified semi-char were the residues of corresponding chars gasified in TGA for 8 h at 800 °C.

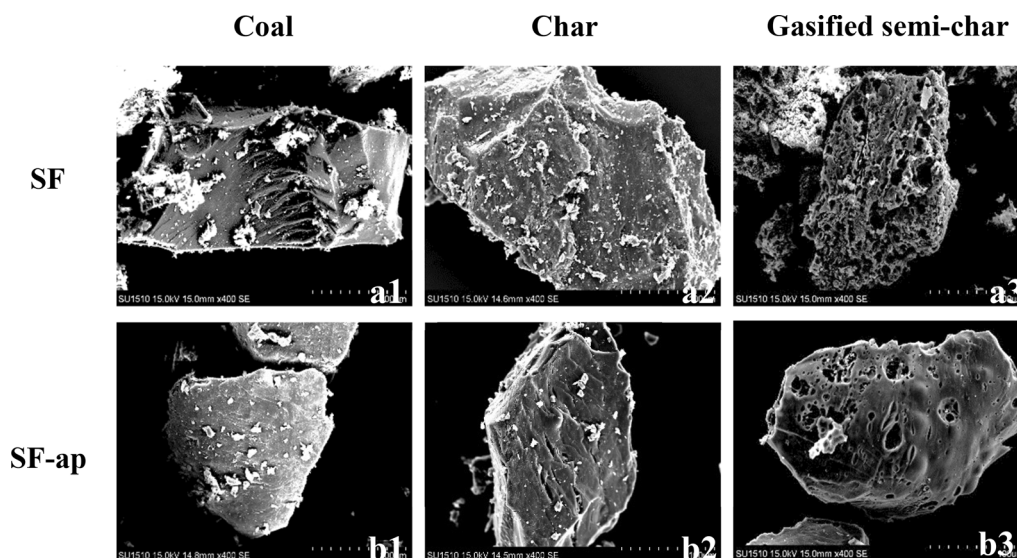


Fig. 1 Morphology of coal, char and gasified semi-char

It could be found that there were fewer small particles sticking on the surface of acid pretreated coal/char, which surface was more luster. Especially after the partial gasification, the surface morphology was significantly different from each other. Some large pores appeared in semi-char with a very smooth surface, as shown in Fig. 1b3, whereas the structure of raw coal char was loose with a layered surface as shown in Fig. 1a3. The carbonaceous structure of gasified semi-char was further discussed in Sect. 3.3.1. Herein, the structure of raw and acid pretreated coal were analyzed. Figure 2a shows the FTIR spectra of SF coal and SF-ap coal. Most of the characteristic peaks were similar, demonstrating that the macromolecular framework structure of coal was not destroyed by HF pickling. For example, a high-intensity band at 1580 cm^{-1} with a weak left shoulder near 1700 cm^{-1} existed, which was attributed to the aromatic C=C stretching vibration and aromatic C=O group, respectively (He et al. 2017). However, a slight change in $2800\text{--}3000$ and $700\text{--}900\text{ cm}^{-1}$ indicated that some aromatic and aliphatic structure had broken (Russo et al. 2014). It was worth noting that the peaks between $1000\text{--}1100$ and $500\text{--}700\text{ cm}^{-1}$ disappeared, which corresponded to SiO_2 and mineral species (Orrego-Ruiz et al. 2011). Figure 2b showed the Raman spectra of raw and acid pretreated coal as well as some parameters from peak fitting. The band ratio between D and G (I_D/I_G) reflected the graphite structure (Zhao et al. 2016). The $I_D/I_{(G+V_R+V_L)}$ was representative of the ratio between large and small aromatic ring (Zhang et al. 2017). The S band reflected the substituted and cross-linking structures (Xie et al. 2019). All these structural parameters increased after the HF pickling. These indicated that the content of large aromatic rings, cross-linking structures and substituted structures increased on the coal surface. In summary, the

mineral species had been removed efficiently after acid pretreatment especially for silica, and the carbonaceous structure on coal surface changed whereas the macromolecular framework structure of coal was stable.

3.2 Slow pyrolysis of raw/pretreated coal

3.2.1 Pyrolysis characteristics

The slow pyrolysis characteristics of raw/pretreated coal are shown in Fig. 3. Two heating rates were taken into consideration. It is reported that the coal pyrolysis mainly goes through three stages (Serio et al. 1987; Wang et al. 2017). Firstly, a mass of aliphatic compounds decomposed thus the weight loss rate increasing. Then, the formation of tar followed, resulting in a decrease in the rate of mass loss. When the temperature further increasing, the secondary peak was noted, which was attributed to the rings condensation and inorganic salt decomposition. In the present work, the primary peak (maximum decomposition rate, R_{max}) of acid pretreated coal was found to decrease by about 10%, and the position of peak (T_{max}) did not move. The decrease of the primary peak suggested that the reduction of aliphatic contents. Another noticeable differences in DTG was the secondary peak of coal at around $700\text{ }^\circ\text{C}$. The acid pretreatment led to the decomposition of inorganic salts in coal, which partly explained the inhibition of secondary peak (Zhou et al. 2016). The minerals removed also inhibited the condensation of aromatic structure (Cheng et al. 2019). Besides, the pyrolysis rate of SF-ap was slightly higher than that of SF below $400\text{ }^\circ\text{C}$, indicating some guest or small molecules with weak bonds were accumulated in coal during HF pickling. On the other hands, the T_{max} increased by $10\text{ }^\circ\text{C}$ at $30\text{ }^\circ\text{C}/$

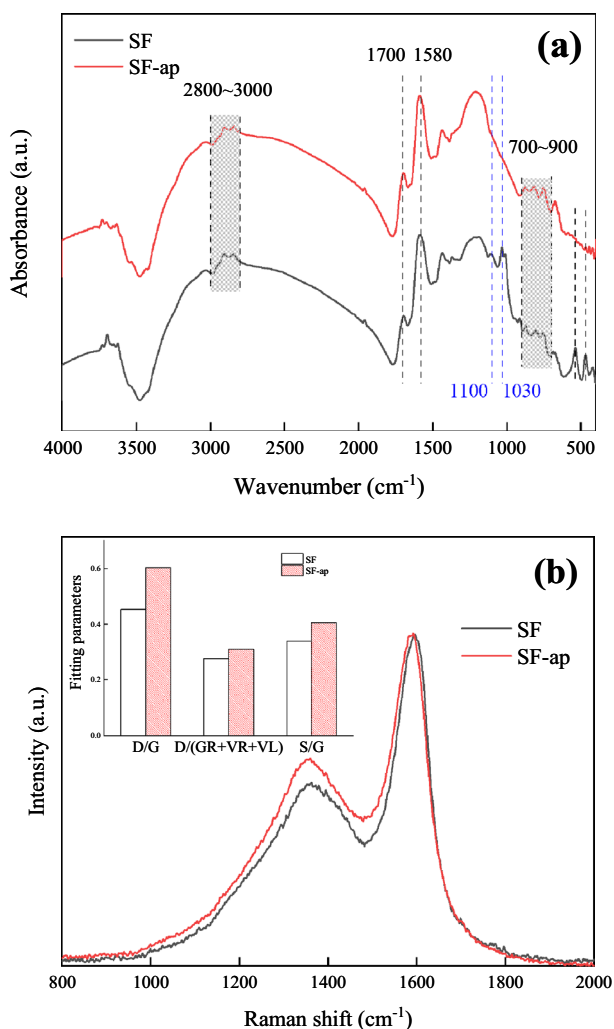


Fig. 2 Spectral analysis of raw and acid pretreated coal **a** FTIR, **b** Raman

min for both coal samples, and the R_{max} increased by 55.9% and 51.2% for SF and SF-ap, respectively. This indicated the raw and pretreated coal was affected by the heat transfer to the same degree. Generally, the pretreatment of HF pickling and the heating rate had limited effect on slow pyrolysis.

3.2.2 Pyrolysis kinetics

For a constant heating rate of β , the Eq. (2) can become

$$\ln\left(\frac{dX/dt}{f(X)}\right) = \ln\left(\frac{A}{\beta}\right) - \frac{E}{RT} \quad (3)$$

Using the Coats–Redfern method, the Eq. (3) can be transformed into

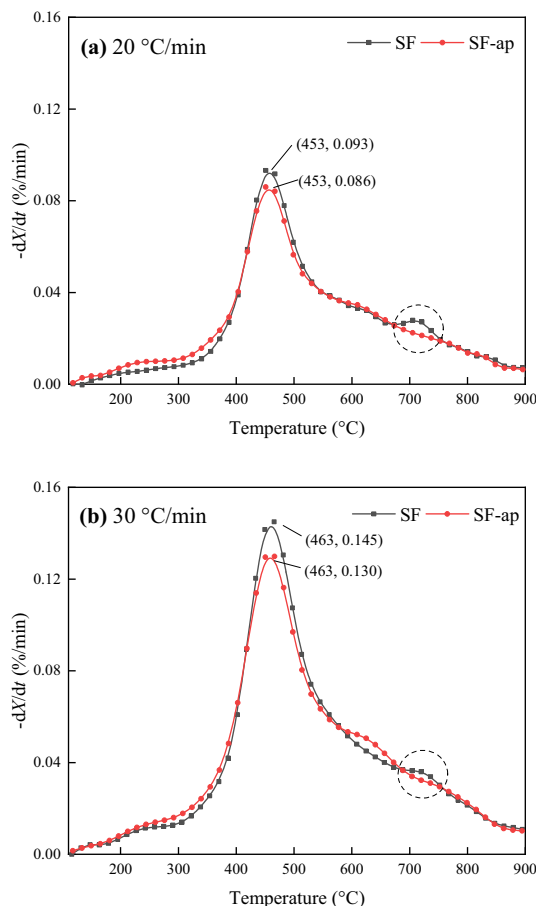


Fig. 3 Pyrolysis rate of coal at different heating rate **a** 20 °C/min and **b** 30 °C/min

$$\ln\left(\frac{g(X)}{T^2}\right) = \ln\left(\frac{AR}{\beta T}\right) - \frac{E}{RT} \quad (4)$$

where $g(X)$ is the integral form of reaction models. The common reaction model are summarized in Table 3, which mainly includes the chemical order and diffusion models (Almazrouei and Janajreh 2020; He et al. 2019a). The master plot $Z(X)$ is used to determine the reaction model, which combines both integral and differential form of the reaction model (Li et al. 2019; Vasudev et al. 2019)

$$\frac{Z(X)}{Z(0.5)} = \frac{f(X)g(X)}{f(0.5)g(0.5)} = \left(\frac{T}{T_{0.5}}\right)^2 \left(\frac{dX/dt}{(dX/dt)_{0.5}}\right) \quad (5)$$

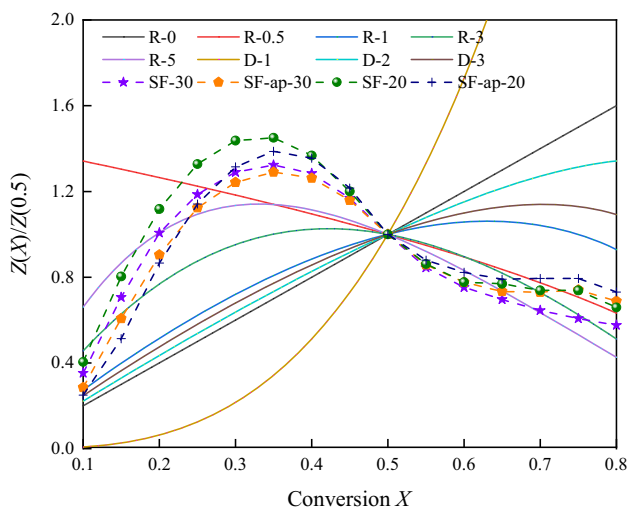
The theoretical curve can be obtained through the left side of Eq. (5), and the right side gives the experimental curve. By comparing the theoretical and experimental curves, the best model can be inferred.

Figure 4 shows the pyrolysis master plot of SF and SF-ap under two heating rates. The heating rate usually has little effect on master plot (Almazrouei and Janajreh 2020; He et al. 2019a). In addition to heating rate, it was found that the pretreatment of HF pickling also had limited effect

Table 3 Brief summary of common reaction models

Item	Models	Symbol	$f(X)$	$g(X)$
Chemical reaction	First order	R1	$1 - X$	$-\ln(1 - X)$
	Reaction order ($n \neq 1$)	R_n	$(1 - X)^n$	$[(1 - X)^{(1-n)} - 1]/(n - 1)$
Diffusion controlled models	1D transport	D1	$1/2 X$	X^2
	2D transport	D2	$[-\ln(1 - X)]^{-1}$	$X + (1 - X)\ln(1 - X)$
	3D transport-spherical	D3	$(3/2)(1 - X)^{2/3}[1 - (1 - X)^{1/3}]^{-1}$	$[1 - (1 - X)^{1/3}]^2$

on master plot or reaction mechanism in this study. However, no typical model can fit the experimental curve well in the whole process. In the early stage of the reaction, the experimental curve was convex. The same trend in master plot was found by Li et al. using biomass (fulvic acid) as the raw material (Li et al. 2019). It was deduced that the coal pyrolysis may follow a higher order reaction according to the trend of the theoretical curves. On the other hand, the segmentation model-fitting method was adopted to calculate the E_a and correlation coefficients. The pyrolysis process was divided into three stages according to Sect. 3.2.1. Figure 5 summarized the results for each pyrolysis step with the heating rate of 20 °C/min. In stage 1, all the tested models had good correlation coefficients. The best model in stage 2 was R2 model. The D3 and some order reactions gave a better fit in stage 3. Moreover, it was found that a higher reaction order gave a larger value of E_a , suggesting some inherent law for the same kinetic model's group (Almazrouei and Janajreh 2020). The similar data proceeding was applied for the pyrolysis with the heating rate of 30 °C/min (Fig. S1). The results showed that the heating rate had little effect on the kinetic parameters obtained by segmentation model-fitting method.

**Fig. 4** Master plot of coal pyrolysis at 20 and 30 °C/min

3.3 Gasification of char from raw/pretreated coal

3.3.1 Gasification characteristics

The gasification properties between SF-(ap)-cs/cl were compared. The isothermal gasification at 800 and 1000 °C are shown in Fig. 6a, b, representing the low and high temperature gasification, respectively. Firstly, the residence time of devolatilization (pyrolysis) had little effect on the raw char reactivity regardless of the gasification temperature variation. Secondly, the reactivity of acid pretreated coal char was related to residence time. The gasification reactivity of SF-ap-cl was lower than that of SF-ap-cs at low temperature. However, the inhibition effect of residence time on char gasification decreased with the increase of gasification temperature. For example, the $X-t$ curve of SF-ap-cs was almost coincided with that of the SF-ap-cl at 1000 °C. Thirdly, although the reactivity of SF-ap-cs/cl were lower than that of SF-cs/cl, the complete reaction time of them were very close (~ 15 min) at 1000 °C, as shown in Fig. 6b. These characteristics were also reflected in non-isothermal gasification, as shown in Fig. 6c. It could be clearly found that the order of reactivity was SF-cs \approx SF-cl $>$ SF-ap-cs $>$ SF-ap-cl. However, the temperature of complete conversion was very close (~ 1000 °C) for these chars. It could be summarized that the difference in reactivity between raw and HF picking coal char became smaller with the temperature increase or reaction process.

Additionally, the gasified semi-char from the interrupted TGA experiment (800 °C, 8 h) was collected to identify the structure evolution during gasification, as shown in Fig. 7. The carbon conversion of SF-cs and SF-ap-cs were approximately 94% and 76% at this point, respectively. The residues morphology was characterized by optical microscope. The gasified semi-char of SF-cs was almost the ash with little carbonaceous as shown in Fig. 7a, whereas residues of the SF-ap-cs still had a lot of carbonaceous particle as shown in Fig. 7b. Meanwhile, the Raman spectra was obtained to analyze the structure evolution during gasification, as shown in the Fig. 7c. The results of the Raman parameters revealed that the

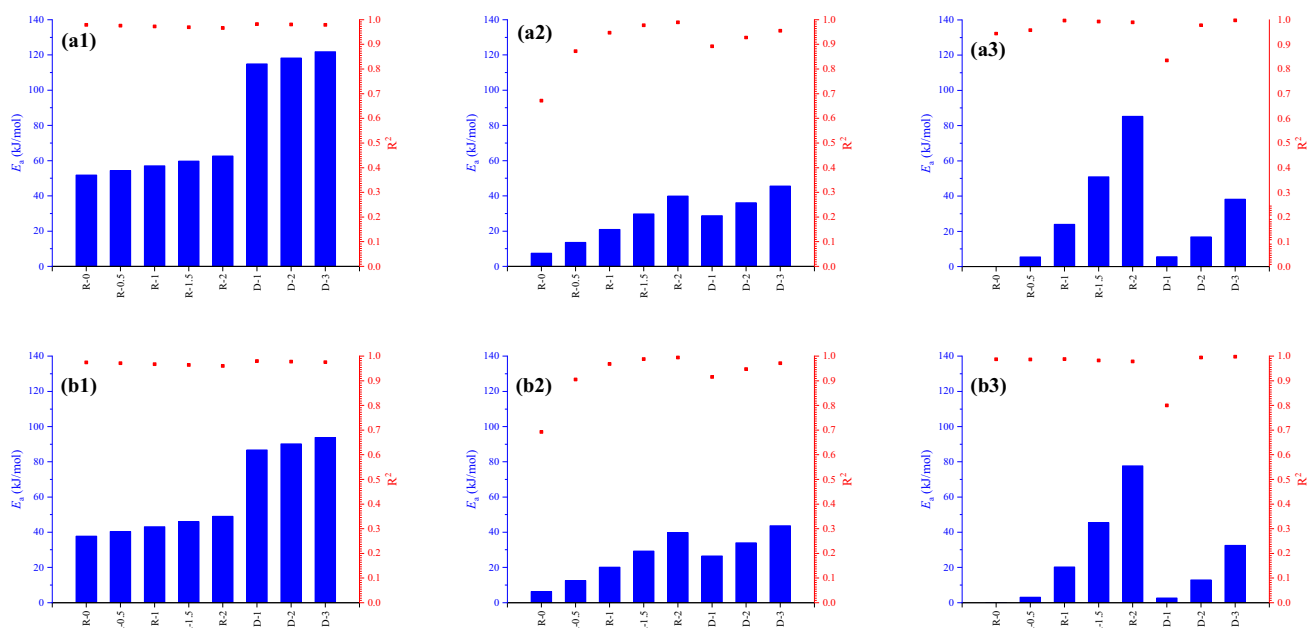


Fig. 5 E_a of **a** SF and **b** SF-ap under the heating rate of 20 °C/min in different pyrolysis stage (1) 350–460 °C, (2) 460–670 °C and (3) 670–800 °C

carbonaceous structures were similar for the two semi-chars, which had gone through the same gasification time. This can be explained by the dispersibility of the particles. It was reported that the particle of pulverized coal can be divided into three types with respect to the minerals, i.e. organic-rich particles, organic particles with included minerals and excluded mineral particles (Zhu et al. 2008). Therefore, the ash content of particle was different to each other in SF-cs char swarms. Herein, most of the particle with relative high ash content had been gasified, while some other particle with little ash was still unreacted. The carbonaceous structures of the two residues were similar to each other accordingly, since they both featured the property of ash-less. Moreover, the mobility is an important parameter for catalyst of gas–solid reaction (He et al. 2020; Neeft et al. 1996). Although the coal ash contained AAEM suggested some catalytic activity, it did not melt and had low mobility under such low temperature. It could be further speculated that the ash in char particle can only accelerate the gasification of itself at low temperature, and had little catalytic effect on other particles.

3.3.2 Gasification kinetics

As discussed in Sect. 3.3.1, the residence time had little effect on SF char gasification reactivity. Hence, the kinetics analysis was carried out for SF-cs, SF-ap-cs and SF-ap-cl. Similar to the kinetic analysis of pyrolysis, the gasification master plot was used for the non-isothermal gasification, as shown in Fig. 8. It could be found that the mechanism of char gasification transformed from reaction order model to

diffusion with the increase of temperature. Specifically, the gasification of SF-cs, SF-ap-cs and SF-ap-cl followed the R-2, R-1 and R-1.5 model in the early stage, respectively. With the gasification proceeding, the D-3 model gave the best fit for all chars. It should be noted that the conversion was related to temperature under the condition of non-isothermal gasification. The mechanism of char gasification usually changes from kinetic control to diffusion control as the temperature increases (Mahinpey and Gomez 2016). The segmentation model-fitting method was not adopted in the present work. Instead, the kinetic parameters were further obtained by analyzing the isothermal gasification.

Inspired by the result of gasification mater plot, the kinetics analysis was performed in low temperature ranges (800–900 °C) and high temperature range (900–1000 °C). Firstly, the model-free method was adopted to calculate the E_a (De Micco et al. 2012). Under the isothermal condition, the integral of Eq. (2) can be expressed as

$$F(X) = \int_0^X \frac{dX}{f(X)} = k_0 e^{-E/RT} t \quad (6)$$

Take the logarithm of both sides of Eq. (6), then

$$\ln t = \ln \frac{F(X)}{k_0} + \frac{E}{RT} \quad (7)$$

Therefore, the E_a at different conversion can be determined from the curve by plotting $\ln t$ against $1/T$. Based on the above derivation, the model-free calculation steps were realized in MATLAB[®] (version R2018b) software. Figure 9 shows the E_a with the conversion of 0.2–0.6,

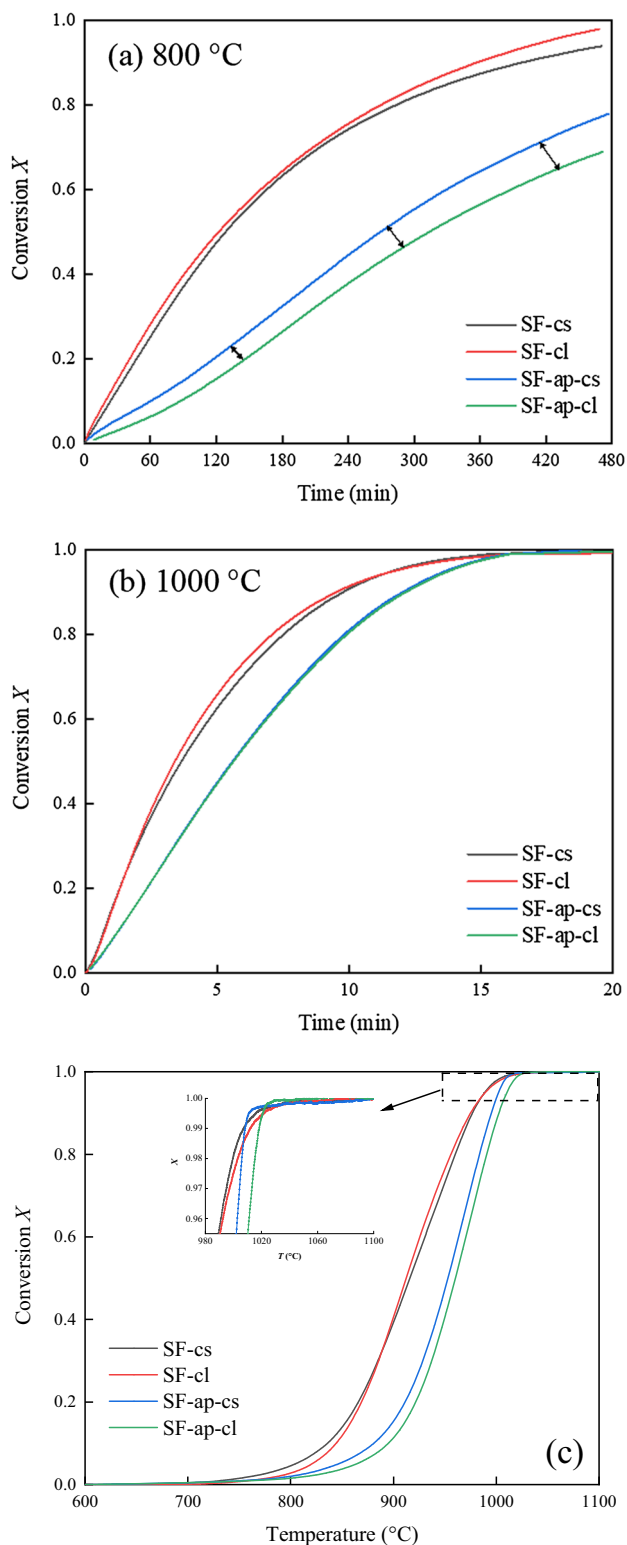


Fig. 6 Char gasification properties at **a** 800 °C, **b** 1000 °C and **c** 5 °C/min

avoiding the interference caused by unstable data collection at the initial and final reaction stage. The value of E_a in low temperature was higher than that in high temperature.

Moreover, the E_a calculated in low temperature range was close to each other (240 kJ/mol). In 900–1000 °C, the order of E_a was SF-ap-cl > SF-ap-cs > SF-cs. Ollero et al. pointed out that the diffusion effect cannot be ignored when the gasification temperature exceeded 900 °C in TGA (Ollero et al. 2002). Herein, the apparent E_a for SF-sc in 900–1000 °C was about half that in 800–900 °C, indicating a significant internal diffusion. However, the diffusion effect was not obvious for the acid pretreated coal char according to the insignificant variation of E_a .

Furthermore, the model-fitting method was performed in low temperature for intrinsic kinetic analysis. In this study, the RPM model was selected for detail analysis, which considered the expansion/overlapping of pores and featured the maximum reaction rate. The structural parameter ψ was obtained by calculating the reduced time ($t_X/t_{0.5}$), which was expressed as follows (Malekshahian and Hill 2011)

$$\frac{t_X}{t_{0.5}} = \frac{\sqrt{1 - \psi \ln(1 - X)} - 1}{\sqrt{1 - \psi \ln(1 - 0.5)} - 1} \quad (8)$$

The curves of reduced time can be considered as another type of master plot. Figure 10 shows the curves of reduced time and the results of structural parameter ψ . It was found that the reaction temperature had little effect on the curves, suggesting the structural parameter ψ should be independent of the gasification conditions. However, the ψ value was affected by the coal pretreatment and pyrolysis conditions. The results show that the ψ value of SF-cs is less than 2, indicating the maximum reaction rate does not exist (Gao et al. 2016; Mahinpey and Gomez 2016). From this perspective, the RPM was not suitable for gasification of the raw coal char. The ψ value of SF-ap-cs and SF-ap-cl were much larger, and the SF-ap-cl with long residence time had largest one. According to Gao et al., the larger ψ value meant the sufficient pore development (Gao et al. 2016). Therefore, it can be concluded that the pore structure of SF-ap-cl would be fully developed since it underwent a long charring time, and the larger ψ value did not imply the higher reactivity. Based on the determined structural parameter ψ , the intrinsic kinetics parameters of SF-ap-cs/cl were calculated through Eq. (9)

$$(2/\psi)(\sqrt{1 - \psi \ln(1 - X)} - 1) = k_{RPM}t \quad (9)$$

Table 4 lists the intrinsic kinetic parameters of acid pretreated coal char. It was found that the k_{RPM} and A of SF-ap-cs were larger than those of SF-ap-cl, indicating a larger frequency of collisions between reactant molecules. However, the k_{RPM} of SF-ap-cs and SF-ap-cl increased by the same factor with the increase of temperature. Thus, the E_a calculated through model-fitting method was almost the same (~ 245 kJ/mol), and it was consistent with the E_a calculated by the model-free method. The variations of

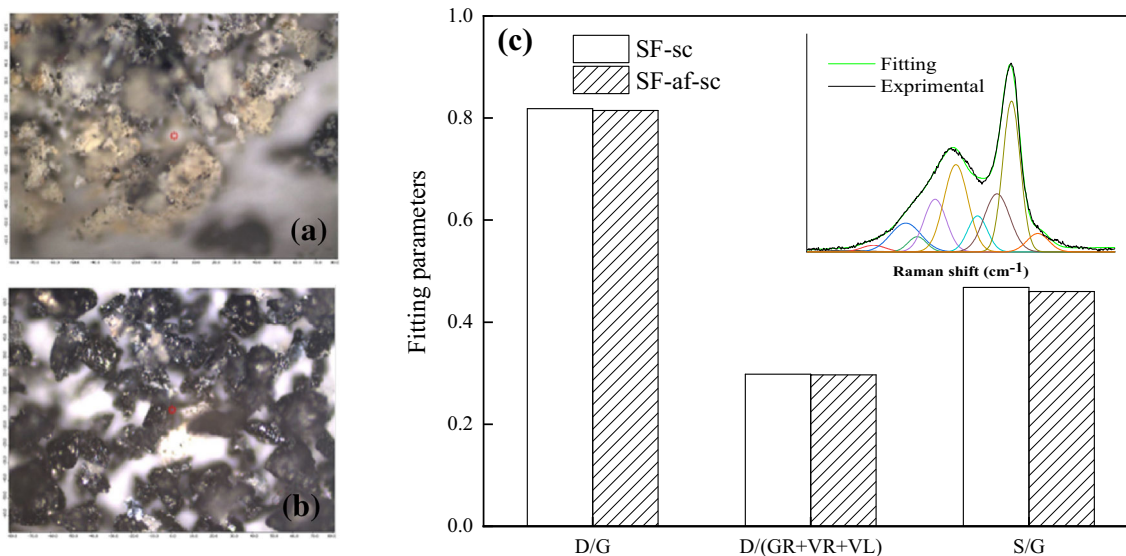


Fig. 7 Semi-gasified char **a** SF-cs particle swarms, **b** SF-ap-cs particle swarms and **c** corresponding Raman parameters

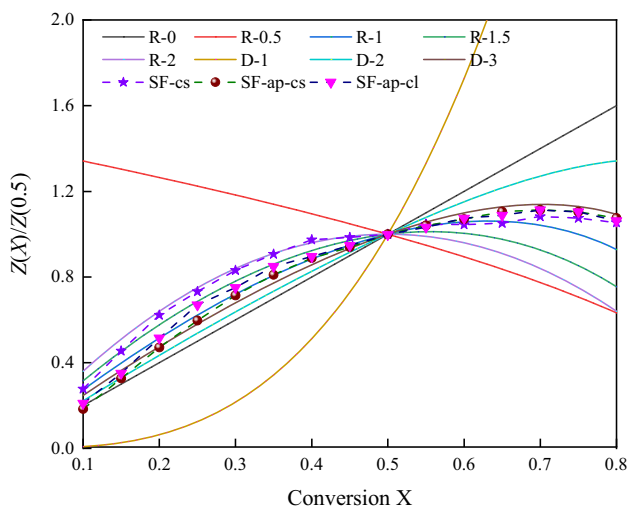


Fig. 8 Master plot of char gasification at 5 °C/min

kinetic parameters explained well to the changes of gasification characteristics (Fig. 6).

4 Conclusions

The ash removal for Shenfu bituminous coal, especially silicon, was achieved by HF pickling in the present work. The reactivity was discussed in detail with an emphasis in kinetics analysis. The following conclusion can be drawn from our study:

- (1) Pretreatment of HF pickling can effectively remove silicon according to FTIR analysis, and the macromolecular framework structure of coal was stable. The results of Raman parameters revealed that the

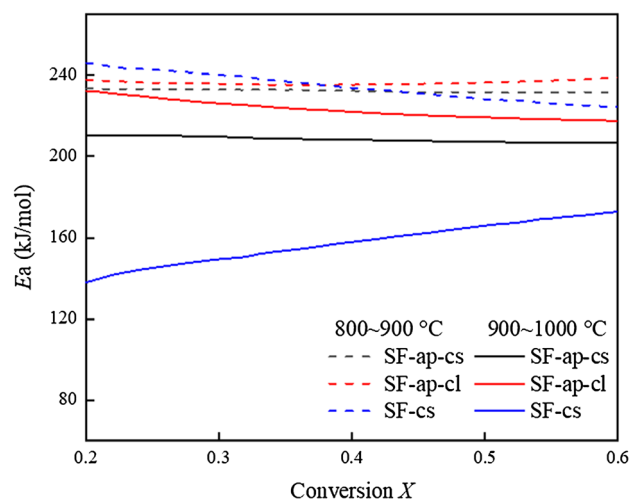


Fig. 9 E_a variation of SF-cs, SF-ap-cs and SF-ap-cl gasification in different temperature range

content of large aromatic rings and the cross-linking structures increased.

- (2) Pretreatment of HF pickling reduced the maximum decomposition rate of coal pyrolysis by about 10%, and suppressed the secondary pyrolysis peak. The pretreatment and heating rate had little effect on slow pyrolysis mechanism according to master plots.
- (3) Pretreatment of HF pickling inhibited the reactivity of char gasification, especially at low temperatures and conversions. However, the intrinsic E_a was approximately 240 kJ/mol for all the chars calculated by model-free and mode-fitting method, respectively. The pretreated coal char with long

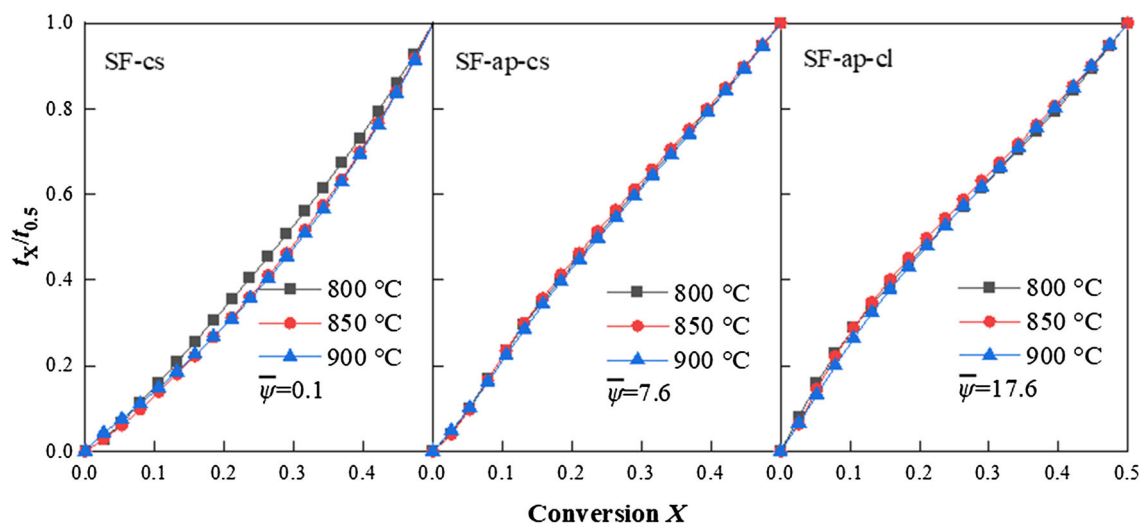


Fig. 10 Determination of structural parameter ψ

Table 4 Kinetic parameters obtained from RPM for acid pretreated coal char

Sample	$k_{\text{RPM}} (10^{-4} \text{ s}^{-1})$			Intrinsic kinetic parameter	
	800 °C	850 °C	900 °C	E_a (kJ/mol)	A (10^7 s^{-1})
SF-ap-cs	0.228	0.732	2.379	245.4	1.976
SF-ap-cl	0.150	0.459	1.558	244.7	1.175

residence time of devolatilization had the larger ψ and smaller A . Besides, the temperature of diffusion control region of acid pretreated coal char was higher than that of raw coal char.

Acknowledgements This work was supported by National Key R&D Program of China (2017YFB0602601) and National Natural Science Foundation of China (21878093).

Open Access This article is licensed under a Creative Commons Attribution 4.0 International License, which permits use, sharing, adaptation, distribution and reproduction in any medium or format, as long as you give appropriate credit to the original author(s) and the source, provide a link to the Creative Commons licence, and indicate if changes were made. The images or other third party material in this article are included in the article's Creative Commons licence, unless indicated otherwise in a credit line to the material. If material is not included in the article's Creative Commons licence and your intended use is not permitted by statutory regulation or exceeds the permitted use, you will need to obtain permission directly from the copyright holder. To view a copy of this licence, visit <http://creativecommons.org/licenses/by/4.0/>.

References

- Almazrouei M, Janajreh I (2020) Model-fitting approach to kinetic analysis of non-isothermal pyrolysis of pure and crude glycerol. *Renew Energy* 145:1693–1708. <https://doi.org/10.1016/j.renene.2019.07.095>
- Bai Y, Lv P, Yang X, Gao M, Zhu S, Yan L, Li F (2018) Gasification of coal char in $\text{H}_2\text{O}/\text{CO}_2$ atmospheres: evolution of surface morphology and pore structure. *Fuel* 218:236–246. <https://doi.org/10.1016/j.fuel.2017.11.105>
- Ban Y et al (2019) Catalytic effect of representative calcium salts on the steam gasification of a Shengli lignite. *Fuel*. <https://doi.org/10.1016/j.fuel.2019.115832>
- Cheng X, Shi L, Liu Q, Liu Z (2019) Effect of a HF–HF/HCl treatment of 26 coals on their composition and pyrolysis behavior. *Energy Fuels* 33:2008–2017. <https://doi.org/10.1021/acs.energyfuels.8b04187>
- Cui Y, Liang J, Wang Z, Zhang X, Fan C, Wang X (2014) Experimental forward and reverse in situ combustion gasification of lignite with production of hydrogen-rich syngas. *Int J Coal Sci Technol* 1:70–80. <https://doi.org/10.1007/s40789-014-0011-8>
- De Micco G, Nasjleti A, Bohé AE (2012) Kinetics of the gasification of a Rio Turbio coal under different pyrolysis temperatures. *Fuel* 95:537–543. <https://doi.org/10.1016/j.fuel.2011.12.057>
- Ding L, Zhou Z, Huo W, Wang Y, Yu G (2014) In-situ heating stage analysis of fusion and catalytic effects of a Na_2CO_3 additive on coal char particle gasification. *Ind Eng Chem Res* 53:19159–19167. <https://doi.org/10.1021/ie503518q>
- Ding L, Gong Y, Wang Y, Wang F, Yu G (2017) Characterisation of the morphological changes and interactions in char, slag and ash during CO_2 gasification of rice straw and lignite. *Appl Energy* 195:713–724. <https://doi.org/10.1016/j.apenergy.2017.03.098>
- Everson RC, Neomagus HWJP, Kaitano R, Falcon R, du Cann VM (2008) Properties of high ash coal-char particles derived from inertinite-rich coal: II. Gasification kinetics with carbon dioxide. *Fuel* 87:3403–3408. <https://doi.org/10.1016/j.fuel.2008.05.019>
- Gao X, Zhang Y, Li B, Zhao Y, Jiang B (2016) Determination of the intrinsic reactivities for carbon dioxide gasification of rice husk chars through using random pore model. *Bioresour Technol* 218:1073–1081. <https://doi.org/10.1016/j.biortech.2016.07.057>

- He X, Liu X, Nie B, Song D (2017) FTIR and Raman spectroscopy characterization of functional groups in various rank coals. *Fuel* 206:555–563. <https://doi.org/10.1016/j.fuel.2017.05.101>
- He Q, Ding L, Gong Y, Li W, Wei J, Yu G (2019a) Effect of torrefaction on pinewood pyrolysis kinetics and thermal behavior using thermogravimetric analysis. *Bioresour Technol* 280:104–111. <https://doi.org/10.1016/j.biortech.2019.01.138>
- He Q, Guo Q, Ding L, Wei J, Yu G (2019b) CO₂ gasification of char from raw and torrefied biomass: reactivity, kinetics and mechanism analysis. *Bioresour Technol* 293:122087. <https://doi.org/10.1016/j.biortech.2019.122087>
- He Q, Yu J, Song X, Ding L, Wei J, Yu G (2020) Utilization of biomass ash for upgrading petroleum coke gasification: effect of soluble and insoluble components. *Energy*. <https://doi.org/10.1016/j.energy.2019.116642>
- Irfan MF, Usman MR, Kusakabe K (2011) Coal gasification in CO₂ atmosphere and its kinetics since 1948: a brief review. *Energy* 36:12–40. <https://doi.org/10.1016/j.energy.2010.10.034>
- Iwaszenko S, Howaniec N, Smoliński A (2019) Determination of random pore model parameters for underground coal gasification simulation. *Energy* 166:972–978. <https://doi.org/10.1016/j.energy.2018.10.156>
- Jayaraman K, Gökalp I, Jeyakumar S (2017) Estimation of synergetic effects of CO₂ in high ash coal–char steam gasification. *Appl Therm Eng* 110:991–998. <https://doi.org/10.1016/j.applthermaleng.2016.09.011>
- Jorjani E, Chapi HG, Khorami MT (2011) Ultra clean coal production by microwave irradiation pretreatment and sequential leaching with HF followed by HNO₃. *Fuel Process Technol* 92:1898–1904. <https://doi.org/10.1016/j.fuproc.2011.05.008>
- Kim G-M, Lisandy KY, Isworo YY, Kim J-H, Jeon C-H (2018) Investigation into the effects of ash-free coal binder and torrefied biomass addition on coke strength and reactivity. *Fuel* 212:487–497. <https://doi.org/10.1016/j.fuel.2017.10.077>
- Kramb J, Gómez-Barea A, DeMartini N, Romar H, Doddapaneni TRKC, Kontinen J (2017) The effects of calcium and potassium on CO₂ gasification of birch wood in a fluidized bed. *Fuel* 196:398–407. <https://doi.org/10.1016/j.fuel.2017.01.101>
- Li T, Song F, Zhang J, Liu S, Xing B, Bai Y (2019) Pyrolysis characteristics of soil humic substances using TG-FTIR-MS combined with kinetic models. *Sci Total Environ* 698:134237. <https://doi.org/10.1016/j.scitotenv.2019.134237>
- Lin L, Strand M (2013) Investigation of the intrinsic CO₂ gasification kinetics of biomass char at medium to high temperatures. *Appl Energy* 109:220–228. <https://doi.org/10.1016/j.apenergy.2013.04.027>
- Lin D, Liu L, Zhao YJ, Zhao Y, Qiu PH, Xie X, Sun SZ (2019) Physicochemical structure characteristics and intrinsic reactivity of demineralized coal char rapidly pyrolyzed at elevated pressure. *J Energy Inst*. <https://doi.org/10.1016/j.joei.2019.10.001>
- Mahinpey N, Gomez A (2016) Review of gasification fundamentals and new findings: reactors, feedstock, and kinetic studies. *Chem Eng Sci* 148:14–31. <https://doi.org/10.1016/j.ces.2016.03.037>
- Malekshahian M, Hill JM (2011) Kinetic analysis of CO₂ gasification of petroleum coke at high pressures. *Energy Fuel* 25:4043–4048. <https://doi.org/10.1021/ef2009259>
- Mi J, Wang N, Wang M, Huo P, Liu D (2015) Investigation on the catalytic effects of AAEM during steam gasification and the resultant char reactivity in oxygen using Shengli lignite at different forms. *Int J Coal Sci Technol* 2:223–231. <https://doi.org/10.1007/s40789-015-0083-0>
- Mishra A, Gautam S, Sharma T (2018) Effect of operating parameters on coal gasification. *Int J Coal Sci Technol* 5:113–125. <https://doi.org/10.1007/s40789-018-0196-3>
- Neef JPA, Makkee M, Moulijn JA (1996) Catalysts for the oxidation of soot from diesel exhaust gases. I. An exploratory study. *Appl Catal B Environ* 8:57–78. [https://doi.org/10.1016/0926-3373\(95\)00057-7](https://doi.org/10.1016/0926-3373(95)00057-7)
- Ning XJ, Liang W, Zhang JL, Wang GW, Li YJ, Jiang CH (2019) Effect of ash on coal structure and combustibility. *Int J Min Metall Mater* 26:973–982. <https://doi.org/10.1007/s12613-019-1812-y>
- Ollero P, Serrera A, Arjona R, Alcantarilla S (2002) Diffusional effects in TGA gasification experiments for kinetic determination. *Fuel* 81:1989–2000. [https://doi.org/10.1016/S0016-2361\(02\)00126-6](https://doi.org/10.1016/S0016-2361(02)00126-6)
- Orrego-Ruiz JA, Cabanzo R, Mejía-Ospino E (2011) Study of Colombian coals using photoacoustic Fourier transform infrared spectroscopy. *Int J Coal Geol* 85:307–310. <https://doi.org/10.1016/j.coal.2010.12.013>
- Royaei MM, Jorjani E, Chelgani SC (2012) Combination of microwave and ultrasonic irradiations as a pretreatment method to produce ultraclean coal. *Int J Coal Prep Util* 32:143–155. <https://doi.org/10.1080/19392699.2012.663024>
- Russo C, Stanzione F, Tregrossi A, Cijolo A (2014) Infrared spectroscopy of some carbon-based materials relevant in combustion: qualitative and quantitative analysis of hydrogen. *Carbon* 74:127–138. <https://doi.org/10.1016/j.carbon.2014.03.014>
- Serio MA, Hamblen DG, Markham JR, Solomon PR (1987) Kinetics of volatile product evolution in coal pyrolysis: experiment and theory. *Energy Fuel* 1:138–152. <https://doi.org/10.1021/ef00002a002>
- Shui H, Li H, Chang H, Wang Z, Gao Z, Lei Z, Ren S (2011) Modification of sub-bituminous coal by steam treatment: caking and coking properties. *Fuel Process Technol* 92:2299–2304. <https://doi.org/10.1016/j.fuproc.2011.08.001>
- Strydom CA, Bunt JR, Schobert HH, Raghoo M (2011) Changes to the organic functional groups of an inertinite rich medium rank bituminous coal during acid treatment processes. *Fuel Process Technol* 92:764–770. <https://doi.org/10.1016/j.fuproc.2010.09.008>
- Vasudev V, Ku X, Lin J (2019) Kinetic study and pyrolysis characteristics of algal and lignocellulosic biomasses. *Bioresour Technol* 288:121496. <https://doi.org/10.1016/j.biortech.2019.121496>
- Vu DL, Lee CG (2016) Oxidation of ash-free coal from sub-bituminous and bituminous coals in a direct carbon fuel cell. *Korean J Chem Eng* 33:507–513. <https://doi.org/10.1007/s11814-015-0164-1>
- Wang J et al (2017) Simulation of pyrolysis in low rank coal particle by using DAEM kinetics model: reaction behavior and heat transfer. *Fuel* 207:126–135. <https://doi.org/10.1016/j.fuel.2017.06.078>
- Xie Y et al (2019) Study on CO₂ gasification of biochar in molten salts: reactivity and structure evolution. *Fuel*. <https://doi.org/10.1016/j.fuel.2019.06.022>
- Zhang Y, Hara S, Kajitani S, Ashizawa M (2010) Modeling of catalytic gasification kinetics of coal char and carbon. *Fuel* 89:152–157. <https://doi.org/10.1016/j.fuel.2009.06.004>
- Zhang L, Li T, Wang S, Song Y, Dong L, Zhang S, Li CZ (2017) Changes in char structure during the thermal treatment of nascent chars in N₂ and subsequent gasification in O₂. *Fuel* 199:264–271. <https://doi.org/10.1016/j.fuel.2017.02.097>
- Zhao Y, Feng D, Zhang Y, Huang Y, Sun S (2016) Effect of pyrolysis temperature on char structure and chemical speciation of alkali and alkaline earth metallic species in biochar. *Fuel Process Technol* 141:54–60. <https://doi.org/10.1016/j.fuproc.2015.06.029>
- Zhao Y, Feng D, Li B, Sun S, Zhang S (2019) Combustion characteristics of char from pyrolysis of Zhundong sub-bituminous coal under O₂/steam atmosphere: effects of mineral matter.

- Int J Greenh Gas Control 80:54–60. <https://doi.org/10.1016/j.ijggc.2018.12.001>
- Zhou L, Zhang G, Schurz M, Steffen K, Meyer B (2016) Kinetic study on CO₂ gasification of brown coal and biomass chars: reaction order. Fuel 173:311–319. <https://doi.org/10.1016/j.fuel.2016.01.042>
- Zhu W, Song W, Lin W (2008) Effect of the coal particle size on pyrolysis and char reactivity for two types of coal and demineralized coal. Energy Fuels 22:2482–2487. <https://doi.org/10.1021/ef800143h>